Preferential {100} etching of boron-doped diamond electrodes and diamond particles by CO_2 activation

Junfeng Zhang,[1] Takaaki Nakai,[2] Masaharu Uno,[2] Yoshinori Nishiki,[2] Wataru Sugimoto[1,*]

1) Faculty of Textile Science and Technology, Shinshu University, 3-15-1 Tokida, Ueda, Nagano 386-8567, Japan
2) Permelec Electrode Ltd, 2023-15 Endo, Fujisawa, Kanagawa 252-0816, Japan

*Corresponding author. Tel: +81-268-21-5455. E-mail: wsugi@shinshu-u.ac.jp

(Wataru Sugimoto)

Abstract

The etching behavior of polycrystalline boron-doped diamond (BDD) electrodes and diamond particles with gaseous CO_2 at 800 and 900 °C was investigated by field-emission scanning electron microscopy, atomic force microscopy and X-ray photoelectron spectroscopy. Polycrystalline BDD (800 ppm), composed of a mixture of cubic {100} and triangular {111} orientated planes, was used so as to pursue the possibility of preferential etching by high temperature CO_2 treatment. Nanometer sized pits were observed on the {100} planes while no change was observable for the {111} planes when the activation temperature was 800 °C. The difference in the etching behavior by CO_2 with regard to the different planes was clarified using diamond particles and comparing with steam activation. The results demonstrate that CO_2 activation leads to preferential {100} etching, whereas steam-activation results in preferential {111} etching.

1. Introduction

The etching of diamond has been studied both from fundamental standpoints [1-7] as well as for practical applications in conductive diamond electrodes [8-12]. The oxidative etching of diamond with O_2 and O_2/H_2O, as well as thermal and hyperthermal atomic oxygen have indicated that the {100} planes are more erosion resistant compared to the {111} planes [1-7]. A similar phenomenon was also observed in the case of H_2O etching of conductive boron-doped diamond (BDD), where steam activation of BDD lead to preferential etching of the {111} planes [13, 14]. In addition to O_2 and H_2O, CO_2 is also a common oxidative etchant. CO_2 activation has been widely used to prepare activated carbon, and is known to lead to activated carbon with a different microstructure compared to steam activation [15-20]. Despite the abundant work on the preparation of activated carbon via CO_2 and steam activation, information on the reaction between CO_2 and diamond is scarce. The oxidative etching of diamond in kimberlite melts at high temperatures and high pressures have shown that oxidation of diamond with CO_2 and H_2O produce different surface features on {111} and {100} faces [21, 22]. To the best of our knowledge, the reaction between CO_2 and boron-doped diamond has not been studied yet. These studies motivated us to study the CO_2 activation of boron-doped diamond. We anticipated that in contrast to the {111} etching observed by steam activation in

boron-doped diamond [13, 14], CO_2 activation may lead to preferential etching of the {100} planes.

Polycrystalline BDD is grown on substrates mainly by CVD processes and consists of randomly oriented crystallites with a mixture of cubic {100} and triangular {111} orientated planes exposed on the surface. Since electrocatalysis and redox reactions are both surface sensitive, BDD with preferential planes exposed to the surface would contribute to a better understanding of the kinetics and electrochemical activity BDD surfaces. The ratio of the exposed planes in BDD electrodes is governed by the CVD conditions and is not easily controlled. For example, highly boron-doped BDD are composed mainly of {111} faces, thus it is difficult to grow diamond films with {100} orientation with high levels of boron doping. The higher level of boron doping in {111} has been suggested to be the cause of higher electron transfer kinetics for redox couples such as $[Ru(NH_3)_6]^{2+/3+}$ and $[Fe(CN)_6]^{3-/4-}$ for {111} than {100} [23, 24].

In this study, CO_2 activation is conducted on polycrystalline boron-doped diamond composed of a mixture of {111} and {100} planes, as well as non-doped diamond crystallites to investigate the etching behavior of doped-diamond surfaces. The etching behavior of different planes is characterized by microscopy and the preferential etching by CO_2 is compared and discussed with activation using steam as the oxidative etchant.

2. Experimental Section

Boron-doped polycrystalline diamond (800 ppm) was synthesized by hot filament-assisted chemical vapor deposition on a Nb substrate (2×2 cm^2) following previously procedures [25, 26]. The electrode with the BDD layer facing up was positioned in a silica boat and set in a silica furnace tube. The furnace temperature was raised to the activation temperature (800 or 900 °C) at a rate of 5 °C min^{-1} under flowing N_2 (99.99995 %). When the activation temperature was reached, N_2 gas was changed to CO_2 gas (200 mL min^{-1}) and held for 2 h. Finally, the samples were cooled down to room temperature under flowing N_2. The samples will be denoted as a-BDD(800°C) and a-BDD(900°C) for BDD activated at 800 and 900 °C, respectively. Steam activation was conducted in a similar fashion to CO_2 activation. Instead of CO_2 gas, ultrapure water (> 18 MΩ cm) was introduced into the silica furnace tube at saturated vapor pressure (40 °C) with N_2 as the carrier gas at a flow rate of 100 mL min^{-1}. Activation using both CO_2 and steam was conducted in an open system with the outlet gas exposed to atmospheric pressure.

The etching of pure diamond by CO_2 activation and steam activation was conducted using as-received diamond crystallites with an average diameter of 300 μm (TOMEI DIAMOND Co. Ltd., IMS-25). The diamond crystallites have a cubo-octahedral structure with well-defined {111} and {100} planes (supplementary material Fig. S1).

A field emission-scanning electron microscope (FE-SEM; Hitachi S-5000) was used for morphological observation. Atomic force microscopy (Bruker, Digital Instruments Nanoscope III ADC 5) was performed in air using silicon cantilevers (Bruker, NCHV-A) and a 130 μm scanner (AS-130V). X-ray photoelectron spectroscopy (XPS) was performed on a Kratos Axis Ultra DLD X-ray photoelectron spectrometer with spectral resolution of approximately 0.8 eV using a standard Mg Kα (1256.6 eV) X-ray source operated at 15 mA and 15 kV. All binding energies were referenced to Au ($4f_{7/2}$) at 83.7 eV. The C1s spectra were fitted with asymmetric mixed Gaussian-Lorentzian sum functions using the XPS peak fitting software XPSpeak (version 4.1). The microstructure of BDD was characterized by Raman spectroscopy (Kaiser Optical Systems, Inc., Raman Microscope System 3000) with a YAG laser (excitation wavelength 532 nm) as the excitation source.

3. Results and discussion

The pristine BDD (800 ppm boron) electrode consists of randomly oriented crystallites with a mixture of cubic {100} and triangular {111} orientated planes exposed on the surface, as shown in Fig. 1a. The {100} and {111} planes can be identified by their shape as well as the difference in contrast in the FE-SEM images. In FE-SEM images obtained with secondary electrons, the cubic {100} planes appear as regions with slightly brighter contrast compared to the triangular {111} planes due to

different electron affinity [27]. Some inhomogeneity in the contrast is observed on the {100} surface, which may suggest of inhomogeneity in the partial atmospheric oxidation of the surface.

A typical FE-SEM image of BDD after CO_2 activation at 800 °C is shown in Fig. 1b (see Supplementary material Fig. S1 for low-magnification images). For a-BDD(800°C), numerous nanopits (5-10 nm) can be observed on the {100} planes, while no etching is evident on the {111} planes, which is more clearly seen in images with higher magnification (Fig. 2). For the steam-activated BDD (Fig. 1c), many pits in the shape of trigon or deformed trigon are formed on the {111} plane, while no etching is evident on the {100} plane (Fig. 1c). FE-SEM images of a-BDD(900°C) reveals progressive etching of the {100} planes at 900 °C forms larger square pits with size of 200-400 nm along the crystal edges (shown with red arrows in Fig. 3), resulting in a macro-porous texture. Etching is so severe at 900 °C, that the {111} planes are no longer able to be distinguish after CO_2 activation. In the case of activated carbon, CO_2 first produces narrow micropores and then the pores are widened as activation progresses [15-20]. If the mechanism of CO_2 activation of BDD is similar to that of activated carbon, then the activation at 900 °C can be attribute to the widening of the nanopits to form large (200-400 nm) square pits.

XPS data was acquired to investigate the change in the carbon species on the surface of BDD (Fig. 4). The relative abundance of the five carbon species obtained from the XPS data is shown in Fig. 5. The percentage of C-C(sp^2) decreased from

8.2 % for pristine BDD to 4 - 5 % for the CO_2-activated BDD, indicating the removal of graphitic impurity by CO_2 activation. This observation was also supported by Raman spectroscopy (see supplementary material). Oxygen functional groups (C-O, C=O) in pristine BDD is due to partial atmospheric oxidation. After CO_2 activation at 800 °C, the relative abundance of C=O increased from 5.6 % to 7.7 % without any obvious change in the C-O. CO_2 activation at 900 °C leads to a further increase in C=O content to 9.2 % and an increase in C-O from 11.8 % to 15.2 % compared to the pristine BDD. The abundance of C-H decreases from 23.7 % for the pristine BDD to 8.8 % for CO_2 activated BDD at 900 °C. C=O is known to form on the {100} plane after oxidation of hydrogen-terminated diamond [28, 29]. A similar trend has been reported for anodic oxidation of BDD, producing C-O and C=O on the {100} plane, while C-O is generated on the {111} plane [30]. Coupled with the FE-SEM images showing the preferential etching of the {100} plane, the increase in C=O can be thus be associated to the partial oxidation of the {100} plane. Although the conditions of oxidation are different, the trend in the kinetics of oxidation by CO_2 activation seems to be similar to oxidation of diamond and anodic oxidation of BDD.

In order to gain more macroscopic insight into the activation process, large non-doped diamond crystallites were subjected to CO_2 activation. Comparative experiments by steam activation was also conducted to clarify the preferential etching behavior. Typical FE-SEM images of diamond particles after CO_2 and steam activation at 900 °C for 2 h are shown in Fig. 6. After CO_2 activation, the {100} plane

is rigorously etched with square pits (around 200 - 400 nm) with pit density of 5.7 pits μm^{-2} (Fig. 6(b)). Etching of the {111} plane is less obvious with some point-bottomed trigons in the size of 100-300 nm (Fig. 6(b')). The trigonal pit density (0.1 pits μm^{-2}) is similar to the defect density of pristine diamond {111} plane, suggesting that the etching occurs at the defect sites. On the contrary, steam activation induces a very different surface feature compared to CO_2 activation. The {100} plane of steam-activated diamond (Fig. 6(c)) has point-bottomed square shaped pits with large size of 0.5 - 2 μm and pit density of 0.8 pits μm^{-2}. The {111} plane has 0.5 - 3 μm sized triangular pits with pit density of 0.13 pits μm^{-2} (Fig. 6(c')). Many steps can be observed on the walls of the triangular pits on the steam-activated {111} plane.

The surface roughness (R) was obtained from AFM images shown in Fig. 7. Before activation, the roughness is $R < 10$ nm for both {111} and {100} planes. For CO_2 activation, increase in roughness of only the {100} plane ($R = 102$ nm) is apparent, and no obvious change can be observed for {111} plane ($R = 10$ nm). Thus CO_2 activation leads to preferential etching of {100} and the {111} plane is resistant to activation. The roughness of the steam-activated {111} plane is $R = 169$ nm, approximately two times higher than steam-activated {100} plane ($R = 89$ nm). Steam activation etches both {111} and {100} plane, although the {111} plane gives a more roughened surface than the {100} plane. Since preferential etching was observed for non-doped diamond, we presume that boron is probably not the active site for etching. However, since the amount of CO_2-etchable {100} planes are less abundant for highly

doped BDDs, it is anticipated that different etching results would be obtained for different doping level. Steam-activation would most likely result in higher degree of etching compared to CO_2-activation for highly doped BDD, and *vice versa* for lower boron-containing BDD.

Based on the obtained results, the CO_2-activation mechanism of polycrystalline BDD is discussed. The oxidative etching of diamond in kimberlite melts at high temperatures and high pressures [21, 22]. In these studies, the relative oxidation rate is different for H_2O or CO_2 and is also sensitive to the diamond plane [21, 22]. The structure sensitive oxidation has been explained by the difference in the position and distance between the open bonds in the diamond lattice is different along the diamond lattice [21, 22]. It is assumed that the preferential oxidation of BDD is similar to that of these high temperature high pressure conditions to some extent. The macroscopic view of the CO_2 activation process of BDD is schematically illustrated in Fig. 8. CO_2 activation at 800 °C leads to mild etching of {100} planes, forming numerous nanopits (5 - 10 nm) on the {100} plane. When the activation temperature is raised to 900 °C, progressive etching of {100} plane occurs with widening of the pores, resulting in the formation of large square pits (200 - 400 nm) along the crystal edges.

4. Conclusion

CO_2 activation of boron-doped diamond and diamond surfaces was conducted and compared with steam-activated surfaces. To the best of our knowledge, this is the first report on the CO_2 activation of diamond or boron-doped diamond under atmospheric pressure. Preferential etching of {100} planes was observed for CO_2 activation at 800 °C, forming numerous nanopits (5 - 10 nm). At this temperature, etching of the {111} surface is minimal. A macroporous surface composed of 200 - 400 nm pits was obtained when the activation temperature was set to 900 °C. Raman and XPS analysis supported the preferential etching of the {100} plane. The preferential etching behavior of boron doped and non-doped diamond is the opposite of what has been observed in the case of steam activation. The results obtained in this work provides a simple and effective method to control the etching of specific surfaces of sp^3 carbon. The preferential etching by CO_2 and steam may allow one to fabricate BDD electrodes with different exposed surfaces at the same doping level, which is difficult to achieve under typical CVD procedures. This work provides a simple and effective method to control the preferential orientation ({111} or {100}) of BDD surface, which can afford a better understanding behind the fundamental electrochemical behavior of specific BDD surfaces.

Acknowledgement

This work was supported in part by a Grant in-Aid for Excellent Graduate Schools, of the Ministry of Education, Culture, Sports, Science and Technology (MEXT), Japan.

Reference

1. Evans T, Sauter H. Etching of diamond surface with gases, Philos Mag 1961;6(63):429-40.
2. De Theije FK, Van Der Laag NJ, Plomp M, Van Enckevort WJP. A surface topographic investigation of {001} diamond surfaces etched in oxygen. Philos Mag A 2000;80:725-45.
3. De Theije FK, Roy O, Van Der Laag NJ, Van Enckevort WJP. Oxidative etching of diamond. Diamond Relat Mater 2000;9(3-6):929-34.
4. De Theije, FK, Van Veenendaal E, Van Enckevort WJP, Vileg E. Oxidative etching of cleaved synthetic diamond {111} surfaces. Surf Sci 2001;492(1-2):91-105.
5. Shpilman Z, Gouzman I, Grossman E, Shen L, Minton TK, Paci JT, et al. Oxidation and etching of CVD diamond by thermal and hyperthermal atomic oxygen. J Phys Chem C 2010;114(44):18996-9003.
6. Paci JT, Schatz GC, Minton TK. Theoretical studies of the erosion of (100) and (111) diamond surfaces by hyperthermal $O(^3P)$. J Phys Chem C 2011;115(30):14770-7.
7. Paci JT, Minton TK, Schatz GC. Hyperthermal oxidation of graphite and diamond. Acc Chem Res 2012;45(11):1973-81.
8. Masuda H, Yanagishita T, Yasui K, Nishio K, Yagi I, Rao TN, et al. Synthesis of

well-aligned diamond nanocylinders. Adv Mater 2001;13:247-9.

9. Terashima C, Arihara K, Okazaki S, Shichi T, Tryk DA, Shirafuji T, et al. Fabrication of vertically aligned diamond whiskers from highly boron-doped diamond by oxygen plasma etching. ACS Appl Mater Interfaces 2011;3:177-82.
10. Yang N, Uetsuka H, Osawa E, Nebel CE. Vertically aligned nanowires from boron-doped diamond. Nano Lett 2008;8(11):3572-6.
11. Takasu Y, Konishi S, Sugimoto W, Murakami Y. Catalytic formation of nanochannels in the surface layers of diamonds by metal nanoparticles. Electrochem Solid-State Lett 2006;9(7):C114-7.
12. Ohashi T, Sugimoto W, Takasu Y. Catalytic roughening of surface layers of BDD for various applications. Electrochim Acta 2009;54(22):5223-29.
13. Ohashi T, Zhang J, Takasu Y, and Sugimoto W. Steam activation of boron doped diamond electrodes. Electrochim Acta 2011;56(16):5599-604.
14. Zhang J, Nakai T, Uno M, Nishiki Y, Sugimoto W. Effect of the boron content on the steam activation of boron-doped diamond electrodes. Carbon 2013;65:206-13.
15. Rodríguez-Reinoso F, Molina-Sabio M, González MT. The use of steam and CO_2 as activating agents in the preparation of activated carbons. Carbon 1995;33(1):15-23.
16. Molina-Sabio M, Gonzalez MT, Rodriguez-Reinoso F, Sepiijlveda-Escribano A. Effect of steam and carbon dioxide activation in the micropore size distribution of activated carbon. Carbon 1996;34(4):505-9.

17. Linares-Solano A, Salinas-Martínez de Lecea C, Cazorla-Amorós D, Martín-Gullón I. Porosity development during CO_2 and steam activation in a fluidized bed reactor. Energy & Fuels 2000;14(1):142-9.
18. Pastor-Villegas J, Durán-Valle CJ. Pore structure of activated carbons prepared by carbon dioxide and steam activation at different temperatures from extracted rockrose. Carbon 2002;40(3):397-402.
19. Román S, González JF, González-García CM, Zamora F. Control of pore development during CO_2 and steam activation of olive stone. Fuel Process Technol 2008;89(8):715-20.
20. González JF, Román S, González-García CM, Valente Nabais JM, Luis Ortiz A. Porosity development in activated carbons prepared from walnut shells by carbon dioxide or steam activation. Ind Eng Chem Res 2009;48(16):7474-81.
21. Fedortchouk Y, Canil D, Semenets E. Mechanisms of diamond oxidation and their bearing on the fluid composition in kimberlite magmas. American Mineralogist 2007;92(7):1200-12.
22. Fedortchouk Y, Manghnani MH, Hushur A, Shiryaev A, Nestola F. An atomic force microscopy study of diamond dissolution features: The effect of H_2O and CO_2 in the fluid on diamond morphology. American Mineralogist 2011;96(11-12):1768-75.
23. Pleskov YV, Evstefeeva YE, Varnin VP, Teremetskaya IG. Synthetic Semiconductor Diamond Electrodes: Electro-chemical characteristics of

homoepitaxial boron-doped films grown at the (111), (110), and (100) faces of diamond crystals. Russ J Electrochem 2004;40:1023-29.

24. Pleskov YV, Evstefeeva YE, Krotova MD, Varnin VP, Teremetskaya IG. Synthetic semiconductor diamond electrodes: Electrochemical behaviour of homoepitaxial boron-doped films orientated as (111), (110), and (100) faces. J Electroanal Chem 2006;595:168-74.
25. Hattori S, Doi M, Takahashi E, Kurosu T, Nara M, Nakamatsu S, et al. Electrolytic decomposition of amaranth dyestuff using diamond electrodes. J Appl Electrochem 2003;33:85-91.
26. Katsuki N, Takahashi E, Toyoda M, Kurosu T, Iido M, Wakita S. Water electrolysis using diamond thin-film electrodes. J Electrochem Soc 1998;145(7):2358-61.
27. Ushizawa K, Watanabe K, Ando T, Sakaguchi I, Nishitani-Gamo M, Sato Y, et al. Boron concentration dependence of Raman spectra on {100} and {111} facets of B-doped CVD diamond. Diamond Relat Mater 1998;7(11-12):1719-22.
28. Pehrrsson PE, Mercer TW. Oxidation of heated diamond C(100):H surfaces. Surf Sci 2000;460:74-90.
29. Pehrrsson PE, Mercer TW. Oxidation of the hydrogenated diamond (100) surface. Surf Sci 2000;460:49-66.
30. Kondo T, Honda K, Tryk DA, Fujishima A. Covalent modification of single-crystal diamond electrode surfaces. J Electrochem Soc

2005;152(1):E18-23.

Figure captions

Fig. 1. Typical HR-SEM images of (a) pristine BDD, (b) CO_2 and (c) steam-activated BDD at 800 °C, respectively.

Fig. 2. Enlarged image of CO_2-activated BDD at 800 °C.

Fig. 3. Typical HR-SEM images of CO_2-activated BDD at 900 °C: (a) high and (b) low- magnification.

Fig. 4. C1s spectra of (a) pristine BDD and CO_2-activated BDD at (b) 800 °C and (c) 900 °C for 2h.

Fig. 5. Relative abundance of the carbon species based on XPS analysis on BDD.

Fig. 6. Typical SEM images of {100} and {111} plane of (a, a') pristine diamond, (b, b') CO_2 and (c, c') steam-activated diamond at 900 °C for 2 h.

Fig. 7. Typical AFM tapping mode images of {100} and {111} plane of (a, a') pristine diamond, (b, b') CO_2 and (c, c') steam-activated diamond at 900 °C for 2 h.

Fig. 8. Schematic illustration of the CO_2-activation process of polycrystalline BDD.

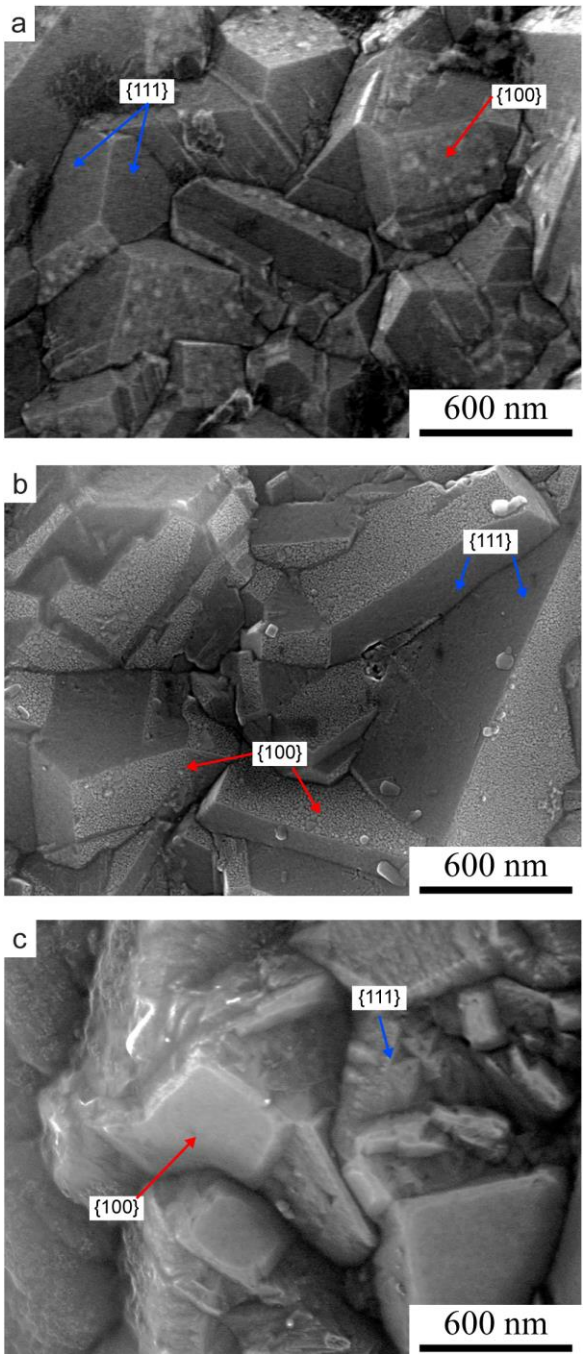

Fig. 1. Typical HR-SEM images of (a) pristine BDD, (b) CO_2 and (c) steam-activated BDD at 800 °C, respectively.

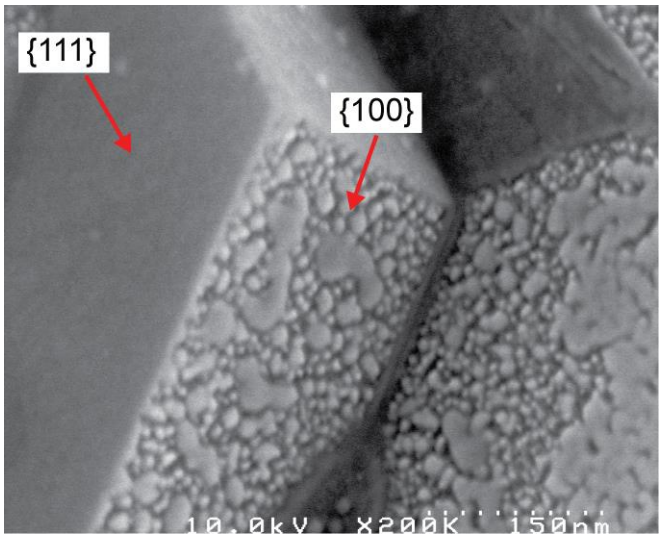

Fig. 2. Enlarged image of CO_2-activated BDD at 800 °C.

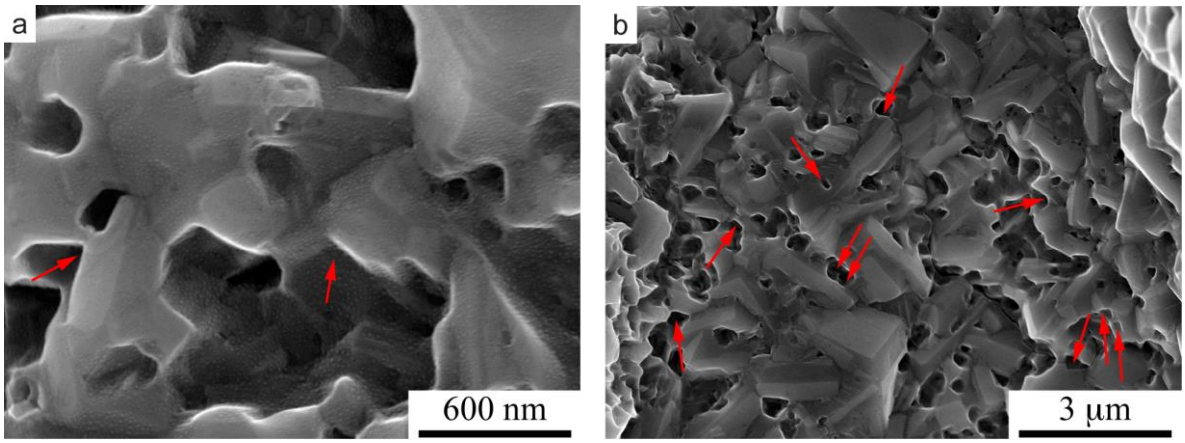

Fig. 3. Typical HR-SEM images of CO_2-activated BDD at 900 °C: (a) high and (b) low-magnification images.

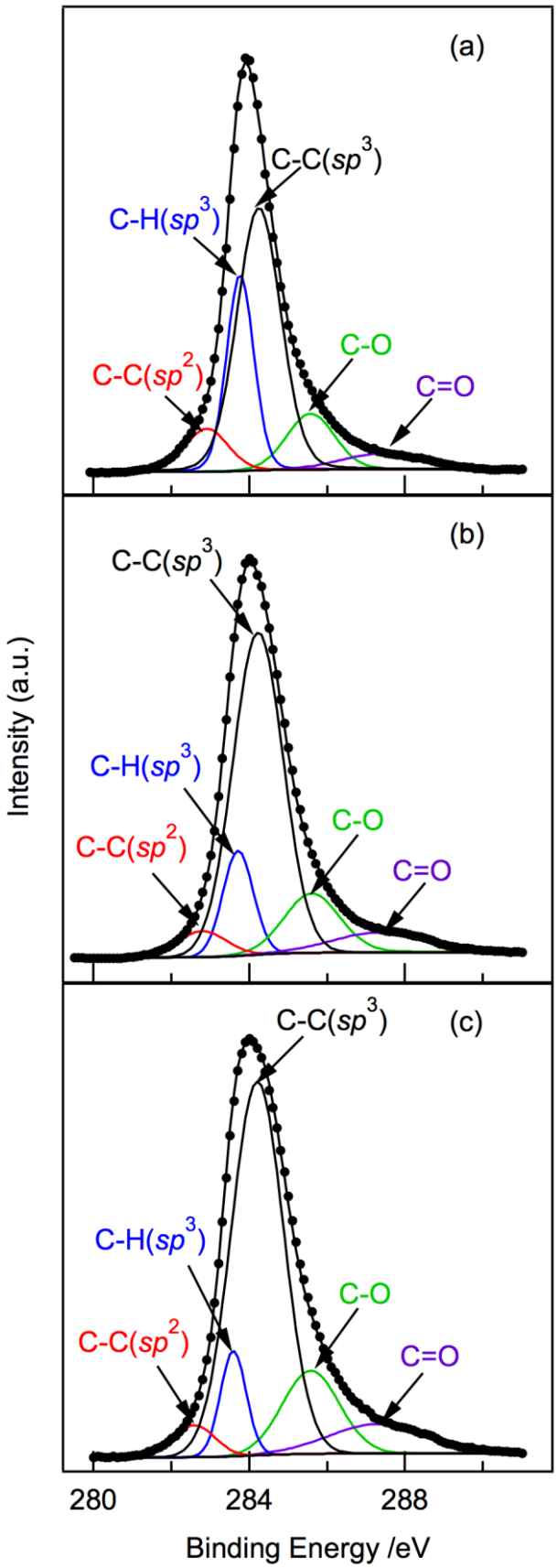

Fig. 4. C1s spectra of (a) pristine BDD and CO_2-activated BDD at (b) 800 °C and (c) 900 °C for 2h.

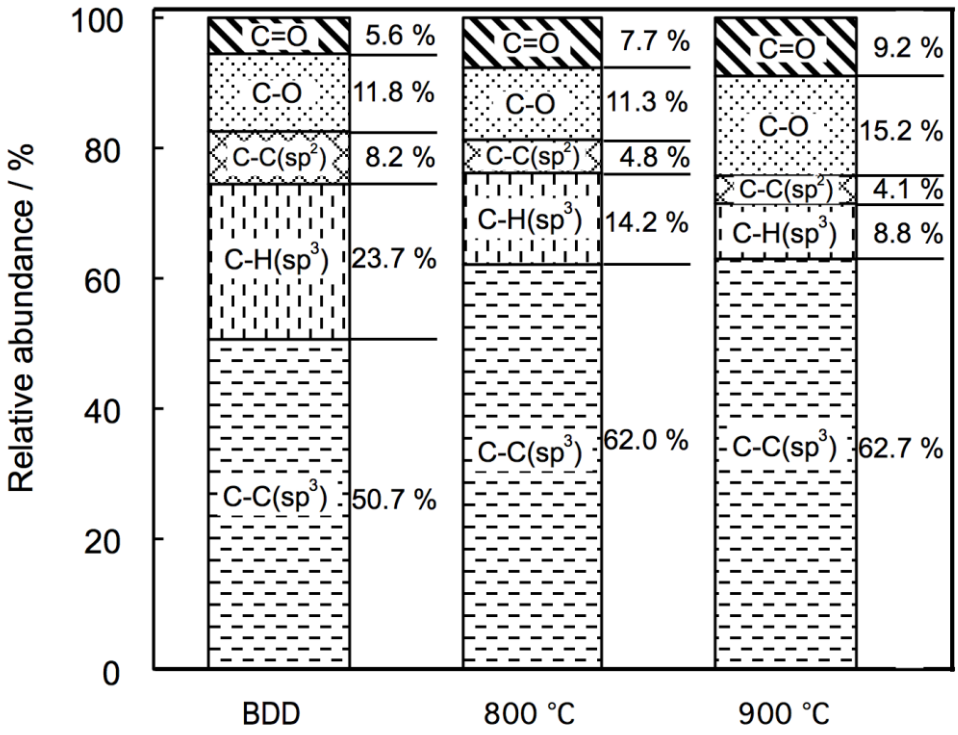

Fig. 5. Relative abundance of the carbon species based on XPS analysis on BDD.

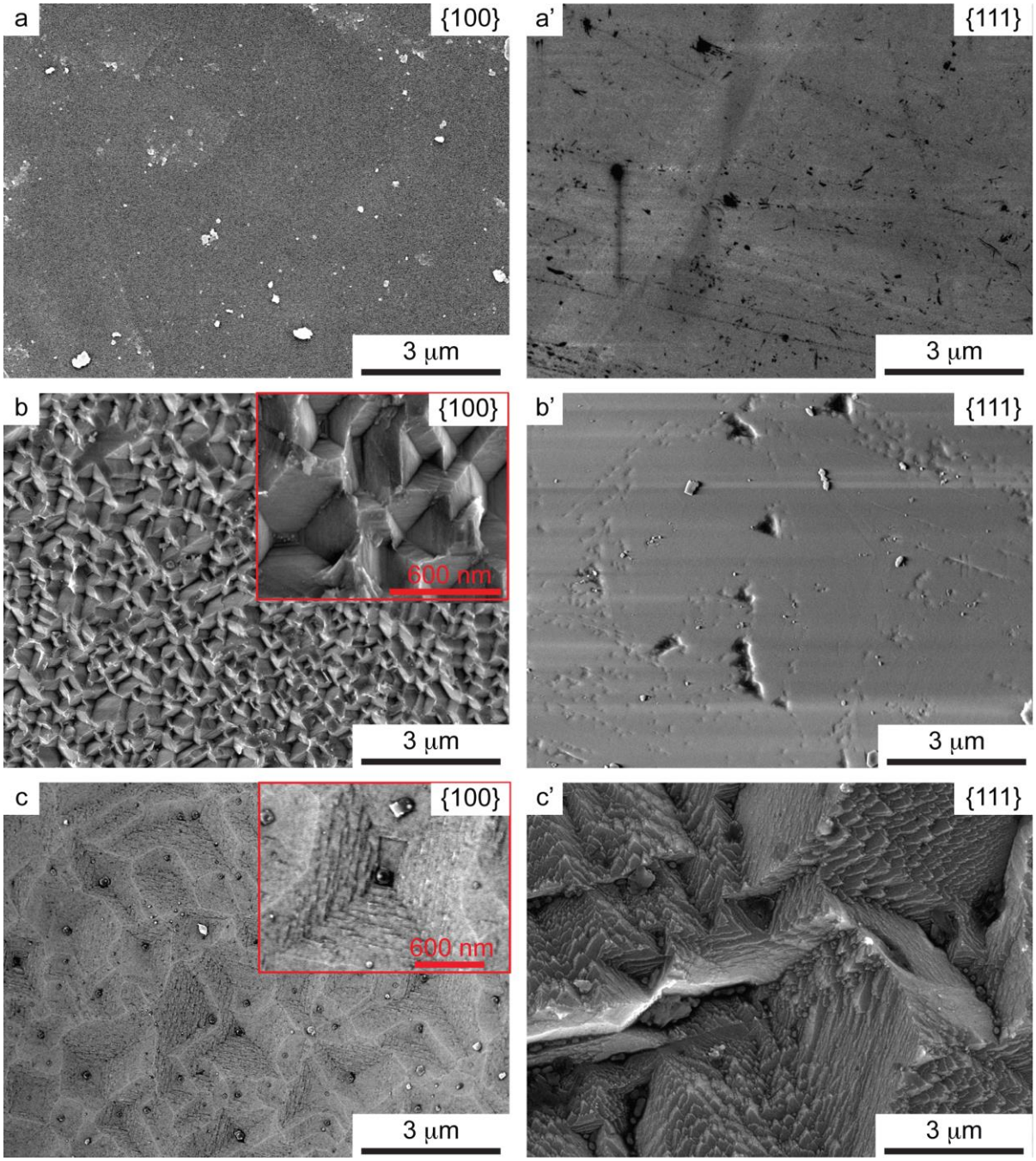

Fig. 6. Typical SEM images of {100} and {111} plane of (a, a') pristine diamond, (b, b') CO_2 and (c, c') steam-activated diamond at 900 °C for 2 h.

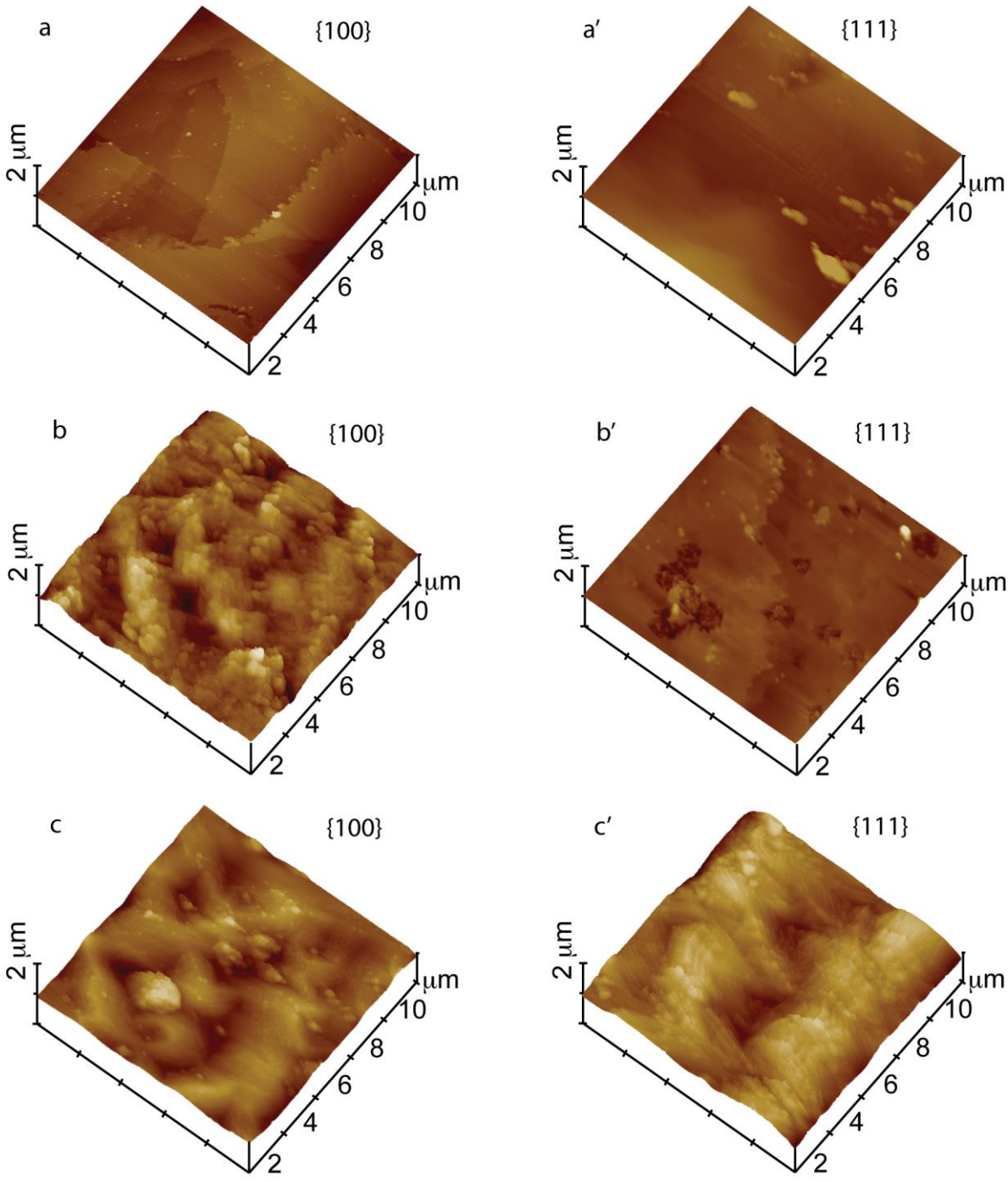

Fig. 7. Typical AFM tapping mode images of {100} and {111} plane of (a, a') pristine diamond, (b, b') CO_2 and (c, c') steam-activated diamond at 900 °C for 2 h.

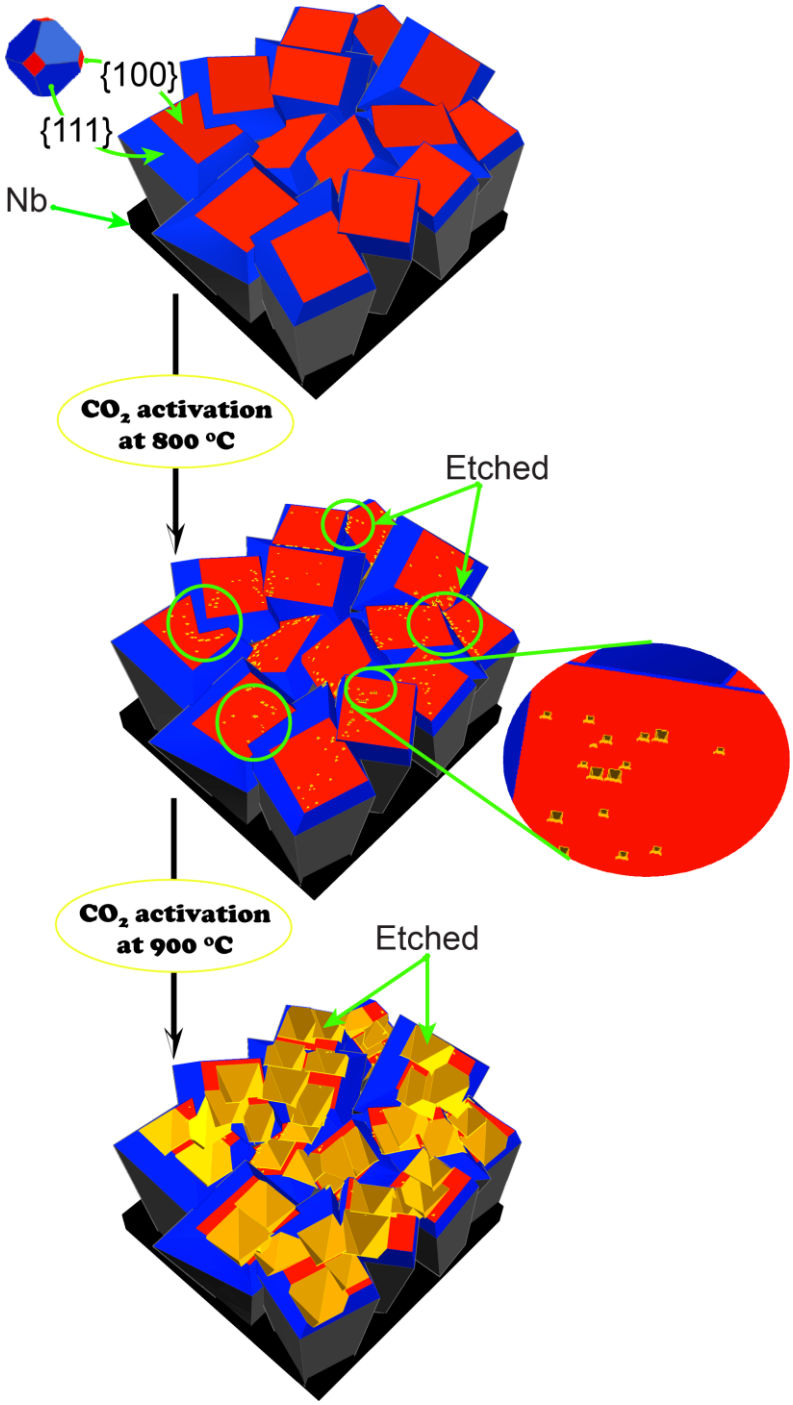

Fig. 8. Schematic illustration of the CO_2-activation process of polycrystalline BDD.